Dynamic field mapping and motion correction using interleaved double spin-echo diffusion MRI

Jana Hutter[1], Daan Christiaens[1], Maria Deprez[1], Lucilio Cordero-Grande[1], Paddy Slator[1], Anthony Price[1], Mary Rutherford[1], and Joseph V Hajnal[1]

Centre for the Developing Brain, King's College London, London, UK
jana.hutter@kcl.ac.uk

Abstract. Diffusion MRI (dMRI) analysis requires combining data from many images and this generally requires corrections for image distortion and for subject motion during what may be a prolonged acquisition. Particularly in non-brain applications, changes in pose such as respiration can cause image distortion to be time varying, impeding static field map-based correction. In addition, motion and distortion correction is challenging at high b-values due to the low signal-to-noise ratio (SNR). In this work we develop a new approach that breaks the traditional "one-volume, one-weighting" paradigm by interleaving low-b and high-b slices, and combine this with a reverse phase-encoded double-spin echo sequence. Interspersing low and high b-value slices ensures that the low-b, high-SNR data is in close spatial and temporal proximity to support dynamic field map estimation from the double spin-echo acquisition and image-based motion correction. This information is propagated to high-b slices with interpolation across space and time. The method is tested in the challenging environment of fetal dMRI and it is demonstrated using data from 8 pregnant volunteers that combining dynamic distortion correction with slice-by-slice motion correction increases data consistency to facilitate advanced analyses where conventional methods fail.

1 Introduction

The unique ability of diffusion MRI (dMRI) to probe microstructural complexity with advanced biophysical modelling techniques facilitates detecting local tissue changes and estimating global connectivity patterns in the brain [6]. Emerging applications such as fetal dMRI may lead to new insights in human brain development, but are complicated by subject motion and image distortion.

Fetal imaging is prone to motion artifacts due to maternal breathing and the fetal movement itself. While frequently employed 2D single shot echo-planar imaging (ssEPI) is quick enough to freeze intra-slice motion, it does not resolve inter-slice motion. As such, the stacks of slices needed to capture whole volumes typically feature inconsistent and highly variable slice locations. Existing techniques reconstruct a motion-corrected volume from these scattered slices using slice-to-volume registration [9]. However, this is challenging at high b-values because the strong signal attenuation and the absence of consistent anatomical features makes these images poorly suited for standard image registration [3].

Geometric image distortion due to magnetic field susceptibility is particularly prominent in EPI imaging due to the low read-out bandwidth. Traditional distortion correction often uses static field maps, either acquired separately or calculated in post-processing from an image pair with reversed phase encoding directions [1]. Furthermore, in fetal applications, changes of the maternal pose due to respiration, as well as the proximity of gas in the maternal bowel result in *time-varying* susceptibility-induced distortion in $\geq 50\%$ of the cases. Traditional techniques assuming static (single time point) field maps are unhelpful in this scenario. The move to 3T for advanced fetal studies has exacerbated these problems, particularly with long scan durations needed for eloquent dMRI data. Eddy current-induced distortion is of minor concern in fetal imaging thanks to the maternal environment.

In this work, we develop an integrated novel acquisition and pre-processing strategy which tries to address these challenges by breaking the fundamental traditional acquisition paradigm of "one volume, one diffusion gradient (b-value and direction)". While conventional dMRI sequentially acquires all slices per volume with a given diffusion weighting, our method interleaves slices with low and high b-values within each slice stack. In addition, acquisition of a second spin-echo with reversed phase encoding at each ssEPI shot facilitates distortion correction for each individual slice [5]. The combination of these elements ensures that there can be low-b information suitable for distortion and motion correction obtained at high temporal resolution, while all required b-values can be obtained for all slices within a super cycle.

2 Methods

2.1 Acquisition protocol

Interleaved diffusion MRI The acquisition yields a sequence of image intensity vectors y_t per slice at time stamps $t \in [1, \ldots, N_d \cdot N_s]$, where N_d specifies the number of diffusion gradients and N_s the number of slices per volume. Each observation y_t is thus described by a geometric index s, a diffusion index d (associated with a b-value and sensitization direction), and its time stamp t.

While in conventional dMRI the N_s slices acquired during each repetition time period, TR, share the same diffusion index d (see Fig. 1a), our technique breaks this continuity (Fig. 1b) and thus reduces the time between sequential low-b data points. An ideal design maximally interleaves low and high b-values for these two goals, but ensures that as many complete volumes of constant-b data are obtained as possible, even if the scan is interrupted or abandoned. Therefore, a super cycle bloc design with length N_i is chosen ($N_i = 5$ in Fig. 1b), where N_i consecutive b-value samplings are interleaved so that all slices are acquired with all diffusion weightings (i.e. b-value shells) after N_i volumes. The number of required blocks depends on the total number of diffusion samples.

Furthermore, the spatial z-location of the slices constitutes a second dimension to be considered. To ensure optimal registration properties, the low b-value

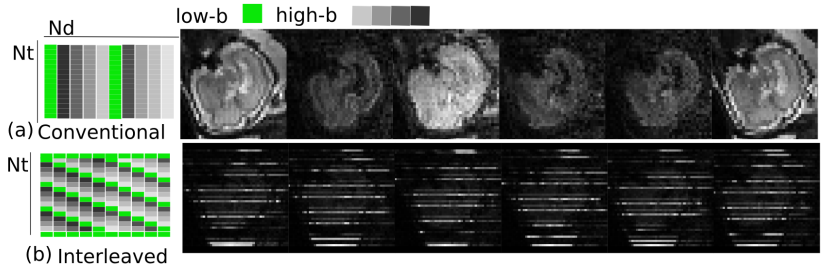

Fig. 1: The schematic diffusion volume vs. slice representation (b-value in color: low-b in green, high-b values in grey.). (a) The traditional one volume, one diffusion gradient sampling approach, and the resulting data reformatted so that the slice direction is along the vertical axis; (b) The proposed sampling with interleaved diffusion sampling for all slices and its corresponding reformatted data. Six consecutive volumes as acquired are shown in both cases.

data was not only spread out maximally in time, to densely sample motion patterns, but also in space to ensure spatial proximity of every high-b slice to a low-b slice. This was achieved by maximizing the inter-slice to inter-shot distances. For example, for the frequently used even-odd slice ordering (0-2-4..1-3-5), this requires that low-b slices are acquired every N_i shots such that the step stride wraps between slice groups. To further facilitate registration, the top and bottom slice of every volume is acquired with $b = 0$ (see Figure 1b). In addition to the main dMRI data set, three additional volumes consisting only of b=0 slices may be acquired in an orthogonal imaging plane to further help volumetric recovery.

Double spin-echo The EPI sequence features a double spin-echo, with the second echo obtained with opposed phase encoding direction (see Fig. 2) for both low and high b-slices. While differing in echo time and thus contrast and signal, the two echoes have matched read-out bandwidth but opposite susceptibility induced distortions. Their temporal proximity under 100 ms and the need for a coherent signal pathway throughout the sequence, ensures that the two images produced per slice can be relied upon to have closely matched (nominally identical) motion states. Susceptibility induced stretching in the first echo (Fig. 2 yellow) corresponds to signal pile-up in the second echo (red). This novel capability, including all required modifications (gradient duty cycle, reconstruction and slice ordering) was implemented on a Philips Achieva 3T scanner.

2.2 Post-processing

The acquired interleaved double spin-echo data of paired phase-encoding and diffusion-weighting form the input data for a bespoke 5 step post-processing framework developed in house using IRTK [10, 7], as illustrated in Fig. 3.

Dynamic distortion correction In Step 1, The acquired double-spin echo interleaved diffusion data is re-ordered to assemble low b-value volumes using

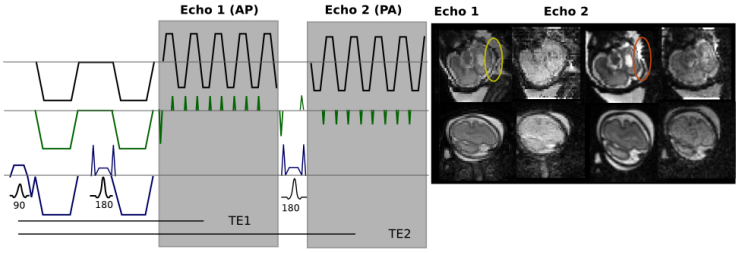

Fig. 2: (a) Simplified sequence diagram of the double spin-echo sequence. (b) Acquired echoes with opposed phase encoding and thus equal-opposite distortions.

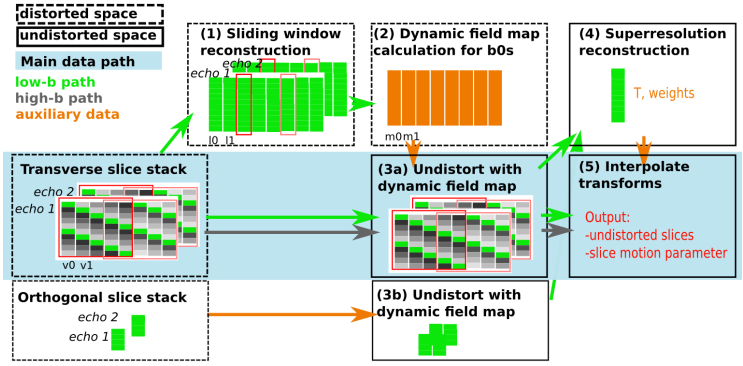

Fig. 3: Illustration of the processing algorithm from the acquired interleaved stacks (left) to the final distortion and motion-corrected dMRI volumes (right). The steps include (1) sliding window volume assembly, (2) dynamic field map calculation, (3) undistortion, (4) superresolution reconstruction [7] and motion correction for low-b slices and (5) propagation of corrections to rest of slice data.

a sliding window approach, thus gathering the temporally closest low-b slices in volumes V_t^{AP} and V_t^{PA} at every time point t. The window size equals the interdiff factor $N_i = 2$, resulting in a maximal temporal distance to measured low-b distortion correction data equal to 2 TR. This data is used in Step 2 to calculate fieldmaps (in Hz) at every time point using FSL `topup` [1].

In Step 3, the temporally closest fieldmap is chosen to correct all slices, both low and high b-values, for distortions. This operation is performed in scanner coordinates and the field maps are converted into displacements in mm taking the bandwidth of the sequence and the EPI factor into account.

Motion correction In Step 4, all the low-b volumes as well as two or three additionally acquired orthogonal low-b volumes are combined as input to the slice-to-volume (SVR) alignment and reconstruction process (as illustrated in [7]) to create a geometrically self-consistent 3D fetal brain volume. The process iterates between a registration step to progressively refine the position estimate of each slice in anatomical space and a super-resolution reconstruction step that uses all newly aligned data to generate a 3D registration target for the next iteration. To

aid convergence, initially each complete low-b volume is registered to the mean of all other low-b volumes, next all slices in the low-b volume are resorted into temporal groups spread over N_i TRs and then registered to the volume, and finally each individual slice is registered to the volume. This allows the position of each slice to be refined while accounting for temporal proximity. The outcome of this processing step is a super-resolved low-b volume, rigid transformation parameters for each individual low-b slice, and a weight assigned to each slice according to how consistent its signals are compared to the co-located data from other aligned slices. The latter information is useful for outlier rejection.

Full data correction In Step 5, all distortion-corrected slices are individually assigned a spatial transformation obtained from interpolating of the transformations for the two closest low-b slices in time. The result of this step is a set of geometrically precise slices with transformations that project them into a self consistent anatomical space—prepared for any post-processing method which can deal with a scattered data space. Direct estimation of derived parameters such as for example the spherical harmonic (SH) coefficients is possible [8].

2.3 Experiments

To illustrate the technique, 8 pregnant volunteers (gestational age 26-34 weeks), were studied using a 32-channel cardiac coil and the proposed interleaved double spin-echo (iDoSE) sequence to acquire 3-shell HARDI data with a total of 49 directions (11 $b = 0$, 8 $b = 400$, 30 $b = 1000\,{}^{\mathrm{s}}/_{\mathrm{mm}^2}$, isotropic resolution $2.2\,\mathrm{mm}^3$, FOV = 320 × 320mm, 34-36 slices per volume, $N_i = 5$, TR = 11 s – 15 s, TA = 12 min, TE = 107 ms for the first echo and 208 ms for the second echo, SENSE factor 2.0, using image-based shimming and fat suppression. In addition, on 4 of these volunteers, sagittal double spin-echo dMRI data with 3 $b = 0$ volumes was acquired with matched imaging parameters.

3 Results

3.1 Dynamic field mapping and motion correction

The dynamic field map calculation based on sparse but frequently acquired $b = 0$ slices provides significant improvement in the presence of motion or varying B0-fields (e.g. as a result of intestinal gas bubbles). The quality of distortion correction is assessed in two settings: (i) with the obtained dynamic fieldmap using the described acquisition and processing steps, and (ii) using a static fieldmap obtained from a non-interleaved acquired double spin-echo pair at the end of the acquisition. After unwarping, the data from both phase encoding directions was vectorized and their correlation coefficient was calculated per diffusion direction. The time series of mean correlations for the low-b volumes is shown in Fig. 4a. The correlation per volume for static (red) and dynamic (green) distortion correction in (b) shows that dynamic field mapping achieves consistently

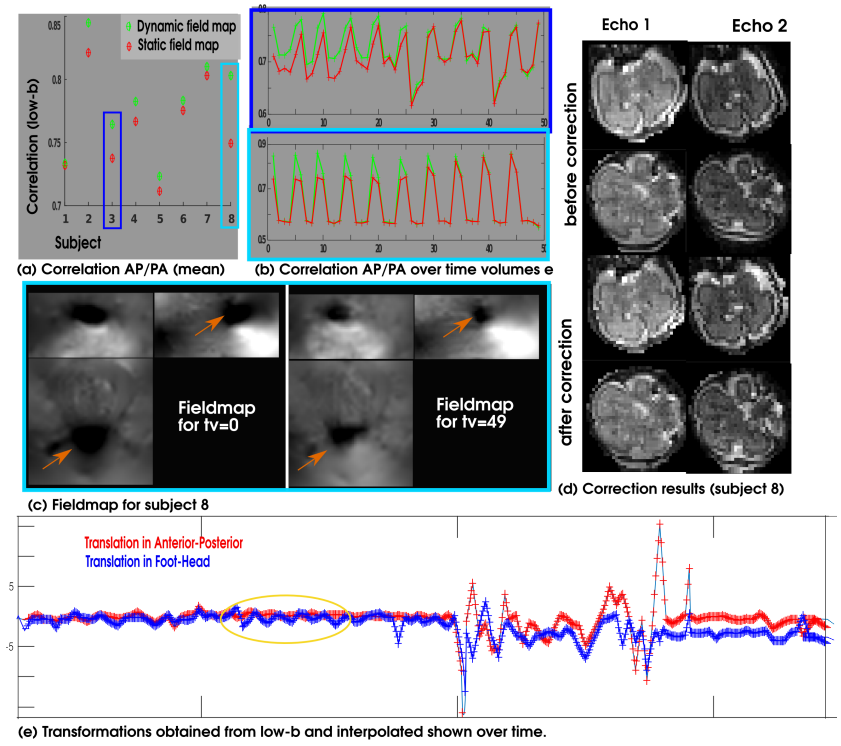

Fig. 4: Results from distortion correction using the dynamic maps. (a) Mean over the correlations between AP/PA images for all low-b volumes are shown for the dynamic field map (green) vs. the static fieldmap acquired at the acquisition end (red). (b) The correlation for every diffusion weighting is shown for both corrections for subject 3 and 8. (c) Fieldmaps from the acquisition start and end, and (d) correction results are shown for subject 8. (e) Translation parameters are shown for anterior-posterior and foot-head direction.

high correlations. The short term oscillations reflect intrinsic variation in correlation caused by the different SNR of low and higher b-value data. Static distortion correction improves towards the end of the series, which is when the static field map was acquired. The upper panel illustrates a case with extensive fetal motion, illustrating improved correction for all volumes in the proposed approach. The lower panel illustrates a case where fetal motion is limited but the fieldmap changes over time due to maternal bowel gas movement, as shown in (c) at the start and end of the sequence. Here, the proposed method significantly improved the consistency of the low-b volumes. Finally, the data from both echoes is shown before and after correction in (d), indicating a high degree of geometrical consistency between the unwarped echoes (a sign of precise distortion correction). The proposed correction framework was successful in all the subjects studied. The SVR algorithm (Step 4-5) using the $b = 0$ slices provided robust motion estimation (Fig. 4e) depicting the breathing cycle of the mother (orange ellipse) in periods of limited fetal motion.

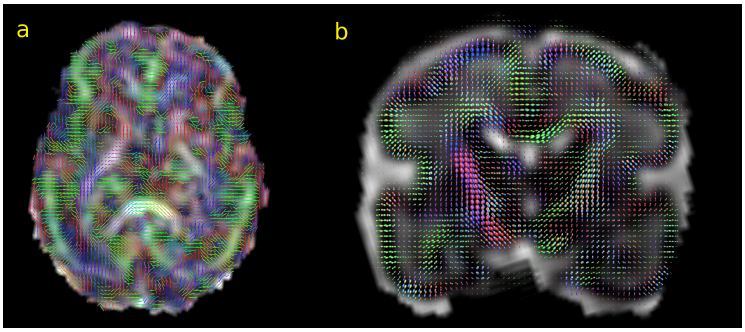

Fig. 5: (a) Axial slice of the fractional anisotropy (FA) map after dynamic distortion and motion correction, overlaid with the principal eigenvectors of the diffusion tensor fit. (b) Coronal slice of a multi-shell multi-tissue decomposition of the same reconstructed data. Vectors and ODFs are coloured according to their direction in the scanner coordinate system, not the subject space.

3.2 Derived quantitative dMRI information

The final dynamic distortion and motion corrected data is suitable for advanced dMRI analysis, including tractography and microstructural modelling. Here, we assess the overall quality of the data using conventional diffusion tensor imaging (DTI) [2] and using multi-shell multi-tissue factorization [4] in two components, associated with brain tissue (SH order 4) and free water (isotropic). Figure 5a shows the fractional anisotropy (FA) image and principal DTI eigenvectors in one fetus. Figure 5b shows tissue orientation distribution functions (ODFs). These results show high anisotropy in the cortex and in maturing white matter structures such as the splenium, as expected in early brain development. The eigenvectors and ODFs are well aligned with developing white matter structures and with cell development perpendicular to the cortical surface.

4 Discussion and conclusion

We presented a method for acquiring and processing dMRI data that is designed to facilitate both distortion and motion correction. The approach allows dynamic distortion correction with a data-derived field map generated every N_i TRs, which for the examples shown means the closest distortion estimate is only 2 TR apart, or about 22-30 sec. Motion correction estimates interpolate between low-b slices that are $(N_i/N_s) \cdot \mathrm{TR}$ apart (1.6 sec for the examples shown), which is well matched to the typical time scale of respiratory motion (5 sec). The second source of motion, fetal motion, is jittered and thus requires more global strategies such as the employed slice-to-volume technique. Inclusion of sufficient low-b slices poses an additional constraint to the optimal sampling scheme, but can include a range of b-values dispersed across lower shells and hence add to the analysis. The choice of the threshold between low b-value (used for active distortion and motion correction) and high-b value (which are to be corrected)

depends largely on the obtained SNR. In the pilot testing done so far the approach proved robust and effective, with clear evidence of both distortion and motion correction in each subject. The full interleaving of high and low b-value slices can also offer benefits in reducing gradient demand, hence improving scan time efficiency. While the introduction of the second echo prolongs acquisition time in standard acquisitions, it combines synergistically with multiband acceleration (MB), where the theoretical TR reduction is not achievable in practice due to the decreased signal. Future work could include advanced transformation interpolation techniques, outlier detection algorithms, and advanced analysis techniques to fully exploit the ancillary second echo too. The fully flexible framework presented proved effective in the fetal dMRI application tested, but is widely generalizable to any diffusion study that includes high b-values. Our processing pipeline will be made available.

Acknowledgements The authors acknowledge funding from the Wellcome Trust, the Developing Human Connectome Project (ERC Grant Agreement no. 319456), the MRC strategic funds (MR/K006355/1) and the NIH Human Placenta Project.

References

1. Andersson J and Skare S: A model-based method for retrospective correction of geometric distortions in diffusion-weighted EPI. NeuroImage 16, 177-199 (2002)
2. Basser PJ, Mattiello J, LeBihan D: MR diffusion tensor spectroscopy and imaging. Biophysical journal 66(1), 259-267 (1994)
3. Ben-Amitay S, Jones DK, Assaf Y: Motion correction and registration of high b-value diffusion weighted images. Magn. Reson. Med. 67(6), 1694-702 (2012)
4. Christiaens D, Sunaert S, Suetens P, Maes F: Convexity-constrained and nonnegativity-constrained spherical factorization in diffusion-weighted imaging. NeuroImage 146, 507-517 (2017)
5. Gallichan D, Andersson J, Jenkinson M, Matthew D, Robson M, Miller K: Reducing Distortions in Diffusion-Weighted Echo Planar Imaging With a Dual-Echo Blip-Reversed Sequence. Magn. Reson. Med. 64, 382-390 (2010)
6. Jones DK: Diffusion MRI: Theory, Methods and Applications. Oxford University Press (2010)
7. Kuklisova-Murgasova M, Quaghebeur G, Rutherford MA, Hajnal JV, Schnabel JA: Reconstruction of fetal brain MRI with intensity matching and complete outlier removal. Medical Image Analysis 16(8),1550-64 (2012)
8. Kuklisova-Murgasova M, Rutherford MA, Hajnal JV: ISMRM 2017, p. 4484
9. Oubel E, Koob M, Studholme C, Dietemann J-L, Rousseau F: Reconstruction of scattered data in fetal diffusion MRI. Medical Image Analysis 16(1):28-37 (2012)
10. Rueckert D, Sonoda L, Hayes C, Hill D, Leach MO, Hawkes DJ: Non-rigid registration using free-form deformations: Application to breast MR images. IEEE Transactions on Medical Imaging, 18(8), 712-721 (1999)